

# HYDRODYNAMICAL SIMULATIONS OF CONVECTION-RELATED STELLAR MICRO-VARIABILITY

Fredrik Svensson and Hans-Günter Ludwig

Lund Observatory, Box 43, 22100 Lund, Sweden

## ABSTRACT

We used a series of CO<sup>5</sup>BOLD hydrodynamical model atmospheres covering stellar objects from white dwarfs to red giants to derive theoretical estimates of the *photometric* and *photocentric stellar variability* in wavelength-integrated light across the Hertzsprung-Russell diagram. We validated our models against solar measurements from the SOHO/VIRGO instrument. Within our set of models we find a systematic increase of the photometric as well as photocentric variability — which turn out to be closely connected — with decreasing surface gravity. The estimated absolute levels of the photocentric variability do not affect astrometric observations on a precision level expected to be achieved by the GAIA mission — with the exception of close-by giants. The case of supergiants remains to be investigated. In view of the ongoing debate about the photometric non-detection of p-modes in Procyon by the Canadian MOST satellite we remark that we obtain a factor of  $\approx 3$  in amplitude between the granular background “noise” in the Sun and Procyon. This statement refers to a particular representation of temporal power spectra as discussed in Sect. 5.

Key words: variability, photometry, astrometry, granulation, hydrodynamics, simulation, oscillations, exoplanets

## 1. INTRODUCTION

The presence of a small-scale time-dependent granulation pattern on the surfaces of late-type stars (see Fig. 1) leads to low-level temporal fluctuations in a star’s total luminosity, apparent position given by its photocenter, (see Fig. 2), and spectroscopically measured radial velocity. During recent years this kind of micro-variability got into the focus of research since it forms an important noise source in searches for solar-like oscillations and exoplanets. This is particularly the case for already operational or upcoming satellite mission like MOST, COROT, and KEPLER; granulation induced micro-variability might also become a limiting factor for precision astrometry missions like SIM and GAIA (Hatzes 2002, Green et al. 2003, Aigrain et al. 2004, Matthews et al. 2004). We performed radiation-hydrodynamics simulations for stellar atmospheres to derive *theoretical*

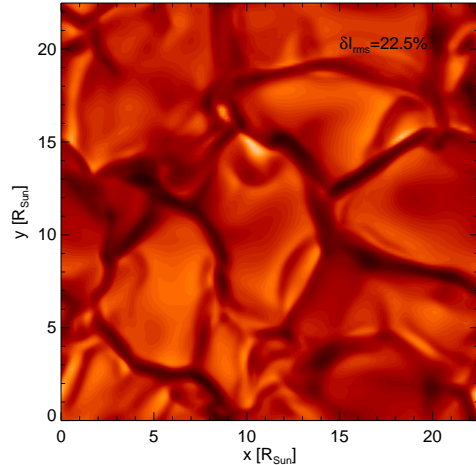


Figure 1. Typical granular intensity pattern from the red giant model sequence. Note the spatial scales.

estimates of the convection-related photometric and photocentric variability across the Hertzsprung-Russell diagram. To our knowledge the work of Trampedach et al. (1998) is the only previous example of such a theoretical effort who studied the brightness and radial velocity variability in the Sun,  $\alpha$  Cen A, and Procyon A.

## 2. CO<sup>5</sup>BOLD RAD.-HYDRODYNAMICS SIMULATIONS

We used the radiation-hydrodynamics code CO<sup>5</sup>BOLD (for further information about the code and applications see Freytag et al. 2002, and Wedemeyer et al. 2004) to construct a series of 3D Cartesian “local-box” model atmospheres. Table 1 summarises the model properties. We calculated three solar models which differ in numerical details. They are used as basic reference and for validating our models by comparison with SOHO/VIRGO observational data. The two models “Procyon A” and “ $\xi$  Hydrae” have parameters close to the actual parameters of the stars they are named after. The other models are not intended to represent particular stars but are generic spanning a large range primarily in surface gravity. Two models are intended to investigate effects of metallicity. Note, that the variation in effective temperature among the models

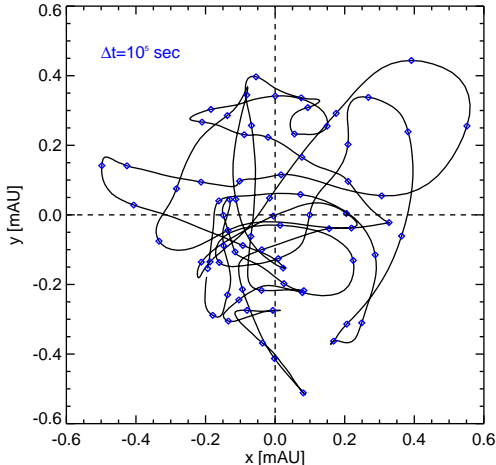


Figure 2. A statistical realisation of the motion of the photocenter in the plane of the sky based on data from the red giant simulation. The time between two diamonds amounts to  $10^5$  s.

is not very large, i.e. the set of models does not fully cover the parameter space. While not apparent from the table significant effort was invested to follow the evolution of the models over long periods of time to ensure statistically representative results.

### 3. FROM SIMULATION BOXES TO STARS

The CO<sup>5</sup>BOLD simulations provide a statistically representative, rectangular patch (or “tile”) of the emergent radiation field and its temporal evolution. In order to derive disk-integrated, observable quantities we have to extrapolate this information to the whole visible stellar hemisphere. To this end we envision the stellar surface being tiled by a possibly large number of simulation patches. Being interested in integrated quantities we can ignore the spatial structure within in a patch and only need to consider averages of the emergent intensity  $I_m$  over the patch surface as a function of time and inclination  $\tilde{\mu}_m = \cos(\vartheta_m)$ . Due to limitations of computing resources the discretisation of the radiation field in solid angle is rather coarse, and usually we have only a total number of inclinations  $M$  (see Tab. 1) of two or three available.

Figure 3 shows an example of a resulting time series with  $M = 3$ . Clearly visible is the effect of limb-darkening and residual intensity fluctuations after averaging over the patch’s surface. The crucial assumption now is that the size of a patch is large enough so that its emission can be considered as statistically independent of all other patches tiling the surface. Moreover, we assume that all patches share the same statistics given by the statistics of the simulated patch. With these assumptions Ludwig (2004) de-

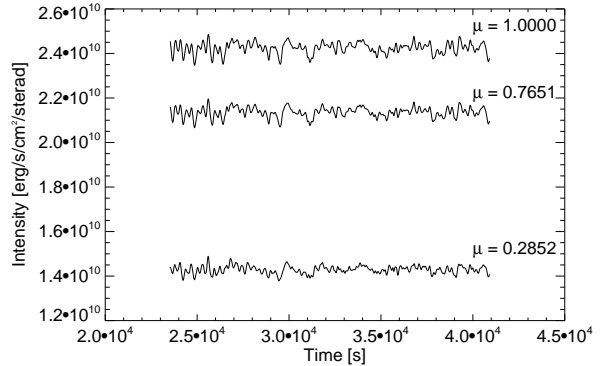


Figure 3. Intensity time series for the three inclinations of model Sun1 showing residual fluctuations and overall limb-darkening.

rived expressions for the statistics of disk-integrated observables which we summarise below.

*Statistics of the photometric variability.* We characterise the photometric variability by the temporal power spectrum of the relative fluctuations of the observable flux  $f$ . The expectation value of a frequency component denoted by  $\hat{f}(\nu)$  is then given by

$$\frac{\langle \hat{f} \hat{f}^* \rangle}{\langle f \rangle^2} = N^{-1} \frac{\sum_{m=1}^M w_m \tilde{\mu}_m^2 \langle \hat{I}_m \hat{I}_m^* \rangle}{\left( \sum_{m=1}^M w_m \tilde{\mu}_m \langle I_m \rangle \right)^2}. \quad (1)$$

Angular brackets denote expectation values, an asterisk the conjugate complex. The sums are discrete analogs of integrals over one half of the total solid angle where  $w_m$  is the integration weight. The numerator expresses that a frequency component of the resulting power spectrum is a  $\tilde{\mu}_m^2$  weighted integral of the frequency components of the individual intensity power spectra. The denominator is essentially the square of the average observable flux. The spectral power density scales inversely proportional to the number of patches  $N$  tiling the visible hemisphere which is given by

$$NA = 2\pi R^2, \quad (2)$$

where  $A$  is the patch surface area and  $R$  is the stellar radius.  $R$  is assumed for the star the atmosphere model is associated with. In this paper we used plausible but to some extent arbitrary values for the stellar radii. For possible later adjustments of the radius one should keep in mind that the power of the photometric fluctuations scales as  $R^{-2}$ . The power spectra presented in this paper are given as spectral density normalised so that the integral between zero and the Nyquist frequency corresponds to the variance of the original signal.

*Statistics of the photocentric displacement.* We characterise the absolute photocentric displacement along an ar-

Table 1. CO<sup>5</sup>BOLD radiation-hydrodynamics model atmospheres: “Model” is a model’s nickname used in this paper,  $T_{\text{eff}}$  the effective temperature,  $\log g$  the gravitational acceleration,  $R$  an assumed stellar radius (not intrinsic to the simulation proper),  $l$  the linear horizontal size of the computational box,  $\tau_c$  the sound crossing time over  $H_p^{\text{surf}}$ ,  $H_p^{\text{surf}}$  the pressure scale height at Rosseland optical depth unity,  $\delta I_{\text{rms}}$  the relative spatial white light intensity contrast,  $N_{\text{obm}}$  the number of equivalent frequency points considered in the solution of the radiative transfer equation (RTE),  $M$  the number of inclinations used in the discretisation of the RTE, “Modelcode” an internal identifier of the model sequence.

Model	$T_{\text{eff}}$ [K]	$\log g$ [cm/s <sup>2</sup> ]	Radius $R$ [Mm]	Box size $l$ [Mm]	$\tau_c$ [s]	$H_p^{\text{surf}}$ [Mm]	$\delta I_{\text{rms}}$	$N_{\text{obm}}$	$M$	Modelcode
Sun1	5 780	4.44	696	5.6	17.8	0.141	0.172	5	3	d3gt57g44n53
Sun2	5 740	4.44	696	18.0	17.8	0.141	0.156	1	2	d3gt57g44sg6
Sun3	5 760	4.44	696	11.2	17.8	0.141	0.176	5	3	gt57g44n67
White Dwarf	12 000	8.00	8.9	7.5 [km]	10.6 [ms]	133 [m]	0.173	1	2	d3t120g80wd1
[M/H] = 0.0	5 170	4.44	696	4.85	16.9	0.128	0.108	5	2	d3gt50g44n01
[M/H] = -2.0	4 730	4.44	696	4.85	17.2	0.118	0.047	6	3	d3ot50g44n01
Procyon A	6 540	4.00	1 460	29.54	49.6	0.391	0.212	1	2	d3gt65g40n2
$\xi$ Hydrae	4 880	2.94	7 340	147.5	513	3.74	0.180	1	2	d3gt50g29n01
Cepheid	4 560	2.00	21 000	2 125	4 310	30.2	0.185	1	2	d3t50g20mm00n2
Red Giant	3 680	1.00	66 300	15 750	40 700	242	0.220	1	2	d3t38g10mm00n2

bitrary axis  $x_{\text{ph}}$  by its standard deviation  $\sigma_{x_{\text{ph}}}$  given to good approximation by

$$\begin{aligned} \sigma_{x_{\text{ph}}} &\approx \frac{R}{\sqrt{6}} \frac{\sigma_f}{\langle f \rangle} = \frac{l}{\sqrt{12\pi}} N^{\frac{1}{2}} \frac{\sigma_f}{\langle f \rangle} \\ &= \frac{l}{\sqrt{12\pi}} \frac{\left( \sum_{m=1}^M w_m \tilde{\mu}_m^2 \sigma_{I_m}^2 \right)^{\frac{1}{2}}}{\sum_{m=1}^M w_m \tilde{\mu}_m \langle I_m \rangle}. \end{aligned} \quad (3)$$

where  $l$  is the linear patch size,  $\sigma_f$  the standard deviation of the observable flux, and  $\sigma_{I_m}$  the standard deviation of the intensity at inclination  $\tilde{\mu}_m$ . The first equality in Eq. (3) expresses a close relationship between the level of fluctuations in the photocentric position and the brightness. This relation carries also over to the temporal power spectrum of  $x_{\text{ph}}(t)$  which is up to a factor  $R^2/6$  identical to the power spectrum of the brightness fluctuations. Remarkably, the last equality in Eq. (3) expresses that  $\sigma_{x_{\text{ph}}}$  is *not* dependent on stellar radius since only quantities intrinsic to the simulation enter. The first equality might suggest the contrary. However,  $\sigma_f/\langle f \rangle$  scales inversely proportional to the radius so that the radius factor cancels. The similarity in the power spectra has the consequence that the characteristic time scale for the fluctuations in photocentric displacement and brightness is the same, namely the evolutionary time scale of individual convective cells. The similarity in the power spectra does not imply that the fluctuations are correlated; it can be shown that photocentric and brightness fluctuations are perfectly uncorrelated.

#### 4. COMPARISON WITH VIRGO OBSERVATIONS

Figure 4 shows a comparison between the disk-integrated, photometric fluctuations derived from our three solar models, and observational data from the VIRGO instrument

on board the SOHO satellite. Our focus is the high frequency region of the solar signal in which granular contributions dominate. The VIRGO power spectrum has been calculated from (level 2) time series data provided<sup>1</sup> by the VIRGO team. Actually chosen was one year of data (1996.5-1997.5) close to solar minimum activity to minimise the possible contribution of activity related variability. Moreover, the plotted power spectrum is based on data of the green channel of the VIRGO three-channel sun-photometer (SPM, see Fröhlich et al. 1997). It has been converted to white light fluctuations by matching (by shifting in power) a corresponding power spectrum based on VIRGO PMO6V-A absolute radiometer data in the frequency range 0.3 to 2.0 mHz. Instead of using the PMO6V-A power spectrum directly this rather involved procedure was necessary since PMO6V-A and SPM power spectra deviate substantially in the high frequency region. The authors found little information about this mismatch in the literature. However, it appears to be consensus that the SPM spectrum reflects the actual solar behaviour (Fröhlich et al. 1997, Andersen et al. 1998), in particular showing the steep (roughly as  $\nu^{-4}$ ) decline at the highest frequencies.

We find a reasonable agreement of the continuous background signal between model predictions and observations between 0.04 and 8.0 mHz. In particular, the background in the p-mode frequency range is matched quite well. The differences among the models can be taken as an estimate of the involved numerical and statistical theoretical uncertainties. We emphasise that the also visible p-mode peaks of the models are *not* expected to match directly the observations since the resonance and excitation properties differ widely between the box models and the Sun.

<sup>1</sup> [http://www.pmodwrc.ch/pmod.php?topic=tsi/virgo/proj\\_space\\_virgo#V](http://www.pmodwrc.ch/pmod.php?topic=tsi/virgo/proj_space_virgo#V)

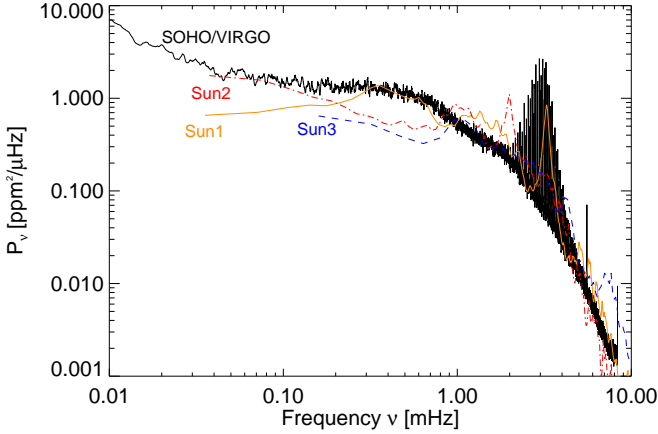


Figure 4. Comparison of power spectra of disk-integrated photometric fluctuations between three solar simulations and observational solar data from SOHO/VIRGO. Note the steep decline in power in the range of the p-mode frequencies.

## 5. TRENDS IN THE PHOTOMETRIC VARIABILITY

Figure 5 shows a comparison of the brightness fluctuations for a sequence of models spanning a range between DA white dwarfs with convective outer envelopes and red giants. The power spectral density  $P_\nu$  is plotted as  $\nu P_\nu$  which makes it independent of the unit in which the frequency is measured. This facilitates the intercomparison among the models where we scaled the frequency with the sound crossing time over a pressure scale height at the surface ( $\tau_c$ ). As evident from Fig. 5 all spectra show a similar shape, and are essentially located in the same scaled frequency range. We find a systematic increase of the photometric variability towards giants. Note, that in fact the square root of the power is plotted in Fig. 5. I.e. our models predict an increase in the *amplitude* by a factor of  $\approx 1000$  between the white dwarf and red giant model.

Our result is in marked contrast to the modelling of Trampedach et al. (1998) who did not find an increase in the granular photometric signal comparing the Sun and Procyon A. However, they pointed out that their time series might have been not long enough to provide sufficient statistics and coverage of lower frequencies. In view of the ongoing debate about the photometric non-detection of p-modes in Procyon by the Canadian MOST satellite (Matthews et al. 2004, Christensen-Dalsgaard & Kjeldsen 2004) we stress that we obtain a factor of  $\approx 3$  in amplitude between the background signal in the Sun and Procyon. This refers to a comparison in a representation like Fig. 5 where differences in power can be essentially described by uniform vertical shift. In a representation in absolute frequencies the power ratio would be frequency-dependent.

By comparing models of similar effective temperature and surface gravity, but different metallicity we find a

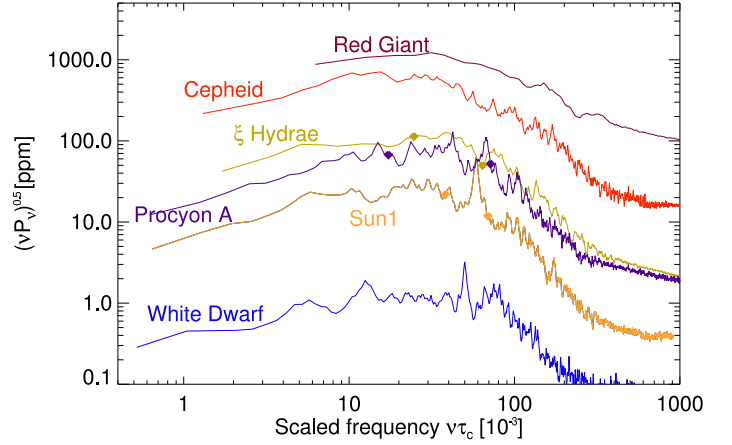


Figure 5. Spectral power density of the brightness fluctuations as a function of scaled frequency  $\nu \cdot \tau_c$ . Diamonds delimit frequency ranges in which p-modes have been detected in radial velocity (Procyon data were taken from Brown et al. 1991,  $\xi$  Hydrae data from Frandsen et al. 2002); observed p-mode frequencies are located in regions with large background power in the models. Note the systematic increase in power with decreasing gravity. The behaviour at scaled frequencies greater than 300 is dominated by the numerics and should be discarded.

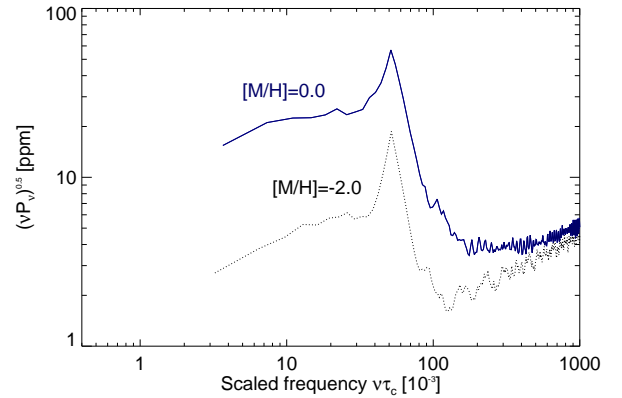


Figure 6. Spectral power density of the brightness fluctuations for two models around  $T_{\text{eff}} = 5000$  K of solar (filled) and 1/100 solar metallicity (dotted). To facilitate comparison the x-axis includes the same range of frequencies as the one in Fig. 5.

decrease of the brightness fluctuations with decreasing metallicity, see Fig. 6. This is in line with expectation that the higher densities encountered at optical depth unity in metal poor models (due to lower overall opacity) leads to smaller convective fluctuations and consequently smaller brightness fluctuations.

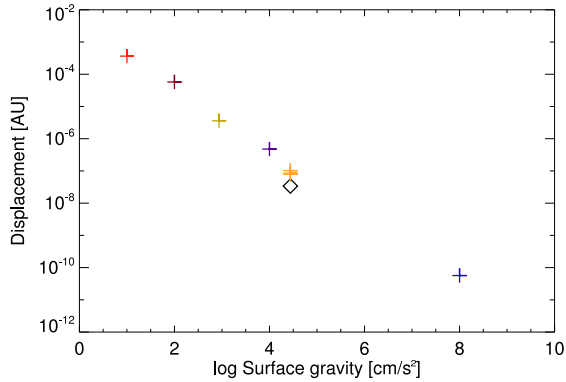


Figure 7. Photocentric displacement as a function of surface gravity. The diamond indicates the metal poor model.

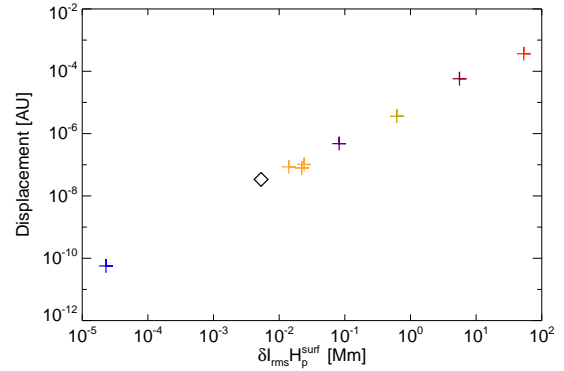


Figure 8. The displacement as function of relative spatial intensity contrast times surface pressure scale height.

## 6. TRENDS IN THE PHOTOCENTRIC DISPLACEMENT

We find an almost perfectly linear relationship between the standard deviation of the photometric displacement and the surface gravity of the models (see Fig. 7). One has to keep in mind, however, that there will be some scatter around this line when considering atmospheres of markedly different effective temperature or chemical composition from the ones considered here. The diamond depicting the metal poor model already indicates this.

Instead of the basic atmospheric parameters ( $T_{\text{eff}}$ ,  $\log g$ , chemical composition), two parameters more closely related to the convection pattern are perhaps physically better suited to describe the functional behaviour of the photocentric displacement — namely the relative spatial intensity contrast  $\delta I_{\text{rms}}$  and the typical size of a convective cell. The size of granular cells is related to the pressure scale height at optical depth unity  $H_p^{\text{surf}}$  (Freytag 2001). Figure 8 depicts the outcome of a test of a relation between photocentric displacement and the product  $\delta I_{\text{rms}} H_p^{\text{surf}}$ : indeed, all models including the metal poor one now follow the same trend. This also indicates that the proportionality to  $g^{-1}$  seen in Fig. 7 is primarily reflecting the systematic increase of granular cell size with decreasing gravitational acceleration.

For our most extreme giant model with  $\log g = 1$  we find a standard deviation of the photocentric position of  $3 \cdot 10^{-4}$  AU or  $0.3 \text{ mas}/D$  [pc] where  $D$  denotes the distance. On a precision level expected to be reached by the GAIA astrometry such a variability does only affect the achievable precision for close-by giants. The situation for supergiants remains to be investigated; a linear extrapolation of the curves shown in Figs. 7 and 8 towards lower surface gravity is unlikely to give a reliable estimate of their photocentric variability since sphericity effects render convection in supergiants markedly different (Freytag et al. 2002) from convection in Cartesian geometry as presented here.

## 7. CONCLUDING REMARKS

We found systematic changes of the convection-induced fluctuations in brightness and photocentric displacement with stellar parameters. The result is a nice example for an application of hydrodynamical model atmospheres (in this respect see Ludwig & Kucinkas, this volume). We would like to emphasise again that we have been considering the contribution of granulation to the stellar variability only. At highest temporal frequencies it is the dominant contributor to the variability. However, at lower frequencies variability related to magnetic activity, spottedness, and rotation dominates, and the level of the fluctuations is likely to be significantly larger than the convective contribution.

### ACKNOWLEDGEMENTS

The authors would like to thank Matthias Steffen for making available one of his solar models (Sun3). HGL would like to thank for the lively as well as insightful discussions with Hans Bruntt and Hans Kjeldsen on solar and stellar high-precision photometry during a visit to the astronomy department of the University of Aarhus. This work benefitted from financial support by the Swedish Research Council and the Royal Physiographic Society in Lund.

### REFERENCES

- Aigrain S., Favata F., Gilmore G., 2004, A&A 414, 1139
- Andersen B.N., Appourchaux T., Crommelynck D., et al., 1998, in: *Sounding solar and stellar interiors* (Poster volume), IAU Symposium 181, eds. J. Provost and F.-X. Schmider, 147
- Brown, T.M., Gilliland, R.L., Noyes, R.W., Ramsey, L.W. 1991, A&A, 368, 599
- Christensen-Dalsgaard J., Kjeldsen H., Nature 430, 29
- Frandsen, S., Carrier, F., Aerts, C. et al. 2002, A&A, 394, L5-L8
- Freytag B., 2001, ASP Conf. Ser. Vol. 223, 785
- Freytag B., Steffen M., Dorch B., 2002, AN, 323, 213
- Fröhlich C., Andersen B.N., Appourchaux T., et al., 1997, Sol. Phys. 170. 1



Green D., Matthews J.M., Seager S., Kuschnik R., 2003,  
ApJ 597, 590  
Hatzes A.P., 2002, AN 323, 392  
Ludwig H.-G., 2004, in preparation  
Matthews J.M., Kuschnik R., Guenther D.B., Walker G.A.H.,  
Moffat A.F.J., Rucinski S.M., Sasselov D., Weiss W.W.,  
2004, Nature 430, 51  
Trampedach R., Christensen-Dalsgaard J., Nordlund Å., Stein  
R.F., 1998, in: *The First MONS Workshop: Science with a  
Small Space Telescope*, eds. H. Kjeldsen and T.R. Bedding,  
Aarhus Universitet, 59  
Wedemeyer S., Freytag B., Steffen M., Ludwig H.-G., Hol-  
weger H., 2004, A&A 414, 1121